Electronic Supplementary Material (ESI) for Physical Chemistry Chemical Physics.

Electronic supplementary information:

The [001]-, [100]- and [110]-orientated α-Si_3N_4 nanobelts with 1 × 1 × 1, 2 × 2 × 1 and 3 × 3 × 1 supercells were constructed by extracting sections of bulk α-Si_3N_4 to examine the effects of section sizes on the energetic stability and photoelectrical properties. Table S1 lists the structural parameters of these supercells. All the surface dangling bonds of α-Si_3N_4 nanobelts were passivated with H atoms. Fig. S1 and Fig. S2 illustrate the [001]-orientated α-Si_3N_4 nanobelts with different section sizes and the [100]- and [110]-orientated nanobelts with 2 × 2 × 1 supercell, respectively.

Table S1 The structural parameters of α-Si_3N_4 nanobelts with different orientations and supercells

Orientation	Supercell	Lattice parameter (Å)			Cell angle (°)		
		a	*b*	*c*	*α*	*β*	*γ*
[001]	1 × 1 × 1	7.77	7.77	5.62	90	90	120
	2 × 2 × 1	15.53	15.53				
	3 × 3 × 1	23.30	23.30				
[100]	1 × 1 × 1	5.62	7.77	7.77	60	90	90
	2 × 2 × 1	11.24	15.53				
	3 × 3 × 1	16.87	23.30				
[110]	1 × 1 × 1	5.62	7.77	7.77	120	90	90
	2 × 2 × 1	11.24	15.53				
	3 × 3 × 1	16.87	23.30				

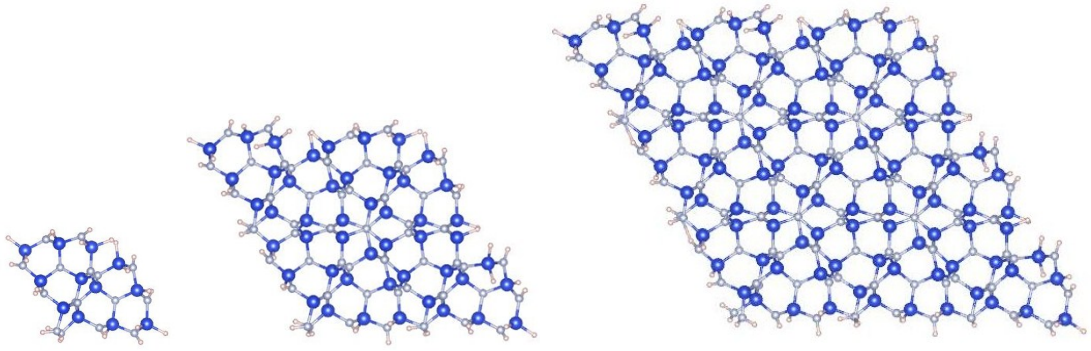

(a) (b) (c)

Fig. S1 Top views of [001]-orientated α-Si_3N_4 nanobelts with different supercells of bulk α-Si_3N_4: (a) 1 × 1 × 1, (b) 2 × 2 × 1 and (c) 3 × 3 × 1. The blue, gray and pink represent Si, N and H atoms, respectively.

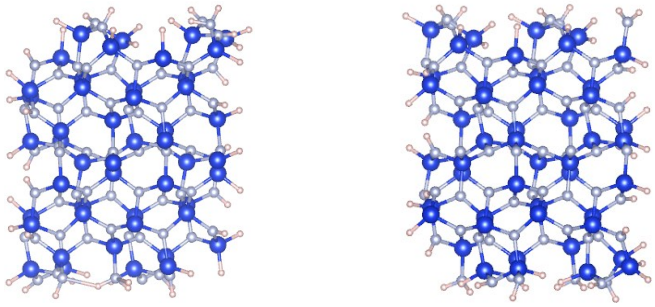

(a) (b)

Fig. S2 Top views of (a) [100]- and (b) [110]-orientated α-Si_3N_4 nanobelts with 2 × 2 × 1 supercell. The blue, gray and pink represent Si, N and H atoms, respectively.

The energetic stability of these α-Si_3N_4 nanobelts was estimated by the total energies per atom, as shown in Fig. S3. The negative values indicate that all these α-Si_3N_4 nanobelts can be synthesized experimentally. The energy decreases with the increase of section size of α-Si_3N_4 nanobelt, indicating the increase of energetic stability.

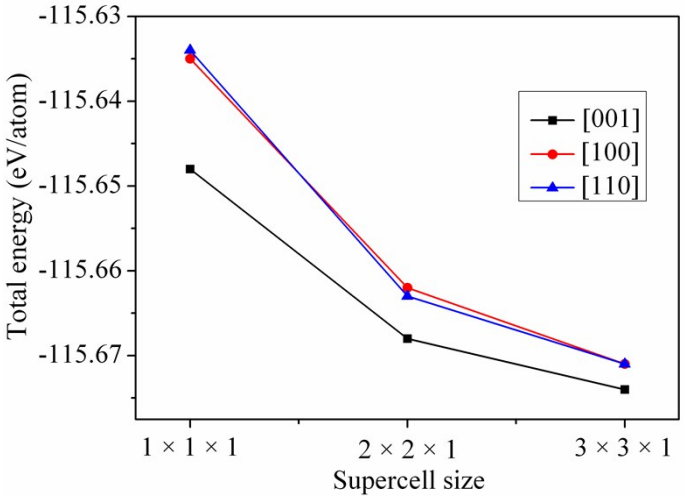

Fig. S3 Total energy per atom as a function of supercell size for the α-Si_3N_4 nanobelts along different directions.

The band structures of α-Si_3N_4 nanobelts with different supercells are shown in Fig. S4. No energy levels cross the Fermi level (set as 0 eV), exhibiting semiconducting characteristics of these nanobelts. The hole and electron effective

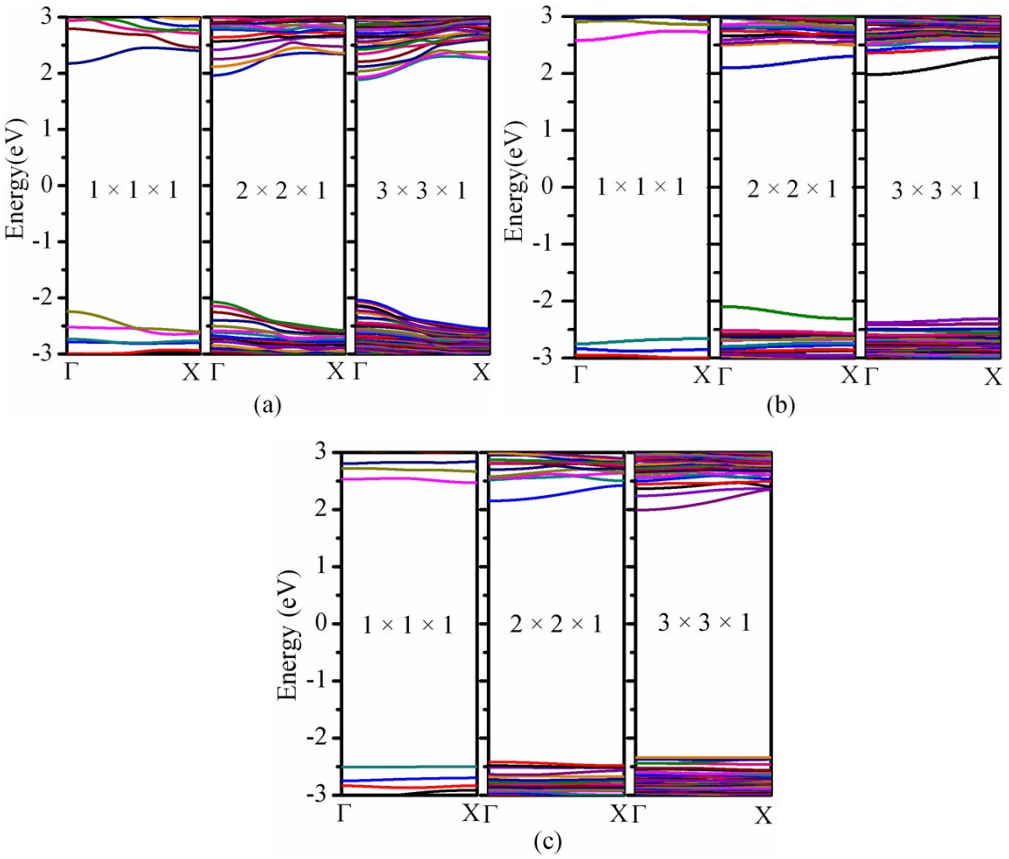

Fig. S4 Band structures of the (a) [001]-, (b) [100]- and (c) [110]-orientated α-Si_3N_4 nanobelts with different supercells.

masses of these α-Si_3N_4 nanobelts are presented in Table S2, where the data before and after "/" represent the hole and electron effective masses, respectively, and the symbols "--" represent the effective masses larger than $5m_0$. It is shown that the section size has little effects on the effective masses of α-Si_3N_4 nanobelts, while the orientation significantly affects them. The band gap values and characteristics based on the band structures are listed in Table S3, where "d" and "i" represent the direct and indirect band gap characteristics, respectively. The band gap values decrease with the increase of section sizes due to quantum confinement effects. Meanwhile, as the supercells increase, the gap value differences decrease. All the α-Si_3N_4 nanobelts exhibit wide band-gap semiconductors with the band gap values larger than 3 eV.

Table S2 The hole/electron effective masses ($\times m_0$)[a] of α-Si_3N_4 nanobelts with different supercells

Supercell	Orientation		
	[001]	[100]	[110]
1 × 1 × 1	-0.75/0.77	--/1.23	--/1.78
2 × 2 × 1	-0.51/0.60	--/2.17	--/1.86
3 × 3 × 1	-0.50/0.61	-4.20/1.71	--/1.64

[a] m_0 is the free electron mass.

Table S3 The band gaps (eV) and characteristics of α-Si_3N_4 nanobelts with different supercells

Supercell	Orientation		
	[001]	[100]	[110]
1 × 1 × 1	4.418(d)	5.243(i)	4.968(d)
2 × 2 × 1	4.034(d)	4.310(d)	4.570(d)
3 × 3 × 1	3.923(d)	4.287(i)	4.332(i)

The partial densities of states (PDOS) of these α-Si_3N_4 nanobelts were calculated to further study their band structures. Similar results were obtained for the [001]-, [100]- and [110]-orientated α-Si_3N_4 nanobelts, so only the representative PDOSs of nanobelts orientating along the [001] direction are displayed in Fig. S5. The VBM and

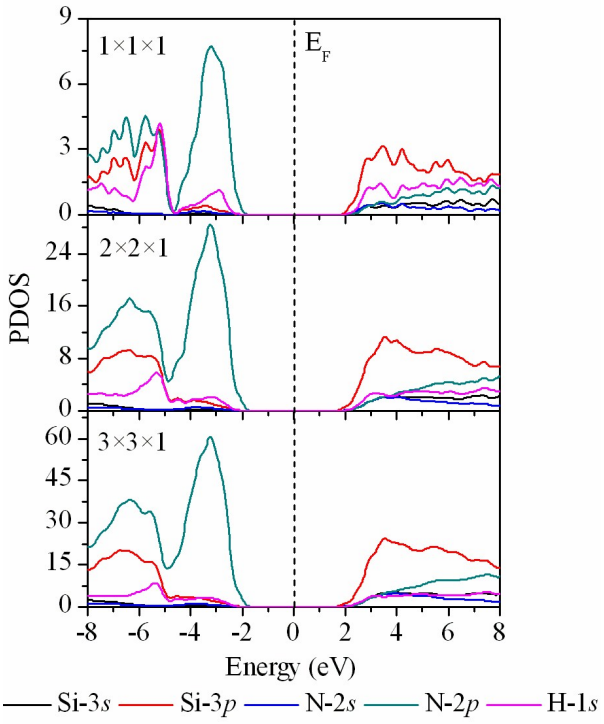

Fig. S5 PDOS of the [001]-orientated α-Si_3N_4 nanobelts with different supercells.

CBM of these α-Si_3N_4 nanobelts with different section sizes are mainly consisted by N-2*p* and Si-3*p* states, respectively, which are similar to the band gap edges of α-Si_3N_4 bulk. The H-1*s* states contribute little to the band gap edges. Moreover, the proportion of H-1*s* states at the VBM and CBM decreases with the increase of section sizes.

The optical properties of α-Si_3N_4 nanobelts with different orientations and supercells were calculated. The linear polarized light was adopted in the directions of parallel ($E // c$) and perpendicular ($E \perp c$) to the nanobelt axis. Fig. S6 displays the imaginary parts $\varepsilon_2(\omega)$ of dielectric functions of nanobelts orientating along the different directions, which possess the similar results. The absorption edge is in the vicinity of 5 eV and red-shifted slightly with the increase of section sizes due to the subtle decrease of band gaps. In addition, as the section size increases, the intensity of dielectric peaks increases. While the supercells increase to 2 × 2 × 1 and 3 × 3 × 1, the number of dielectric peaks decreases, and the peak shapes and locations tend to be similar to each other. The two well-resolved peaks locate at about 8.5 eV and 10.5 eV, and one peak with a broad distribution appears in the range of 15~17 eV. According to the PDOS in Fig. S5, these peaks mainly correspond to the transitions of N-2*p* electrons in the valence band to Si-3*p* electrons in the conduction band due to the few contributions of H-1*s* states to the band gap edges. For the α-Si_3N_4 nanobelt with 1 × 1 × 1 supercell, the newly appearing peaks may originate from the electron transitions of H-1*s* states in the valence band to Si-3*p* states in the conduction band due to the higher proportion of H-1*s* states at the band gap edges.

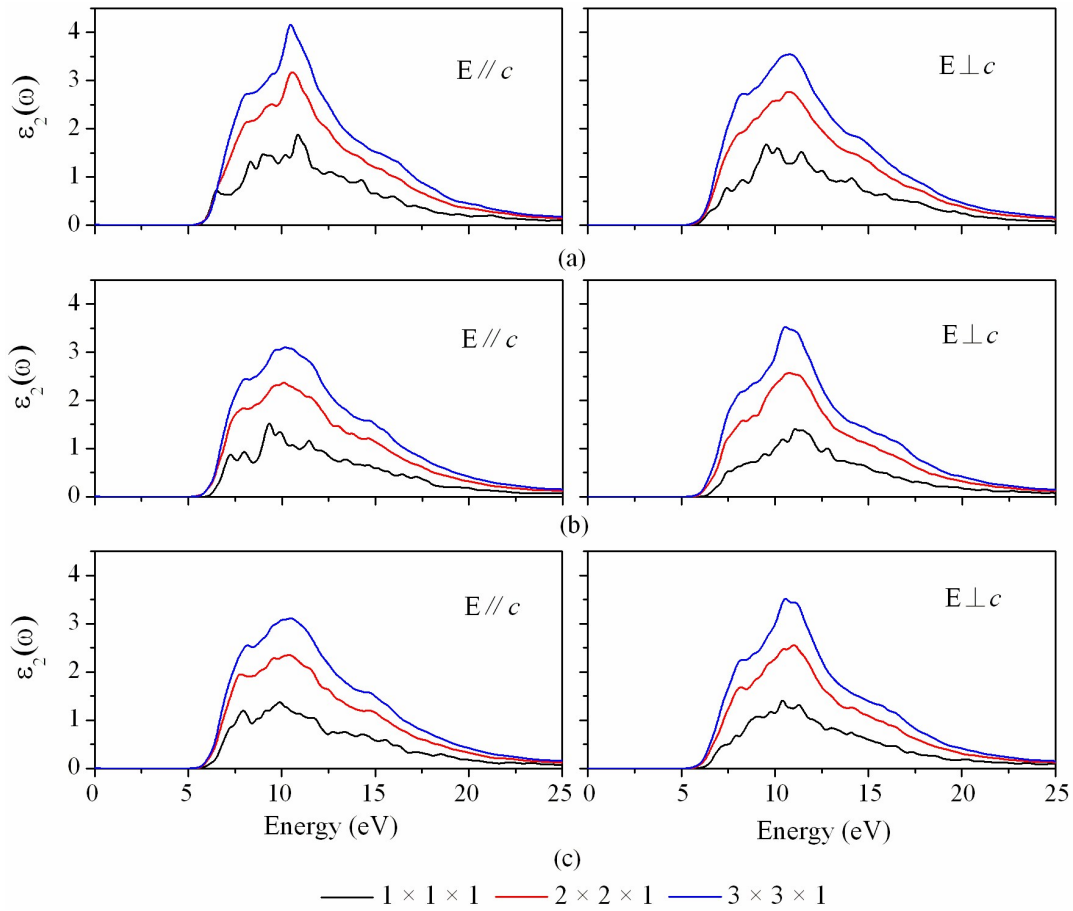

Fig. S6 Imaginary parts $\varepsilon_2(\omega)$ of the dielectric functions of the (a) [001]-, (b) [100]- and (c) [110]-orientated α-Si_3N_4 nanobelts with different supercells.

The real parts $\varepsilon_1(\omega)$ were obtained from the imaginary parts $\varepsilon_2(\omega)$, as shown in Fig. S7. In the energy rangy of 0~11 eV, $\varepsilon_1(\omega)$ increases with the increase of section size, but at the energies higher than 11eV, the opposite is true. Affected by the imaginary parts, the number of $\varepsilon_1(\omega)$ peaks also decreases as the supercells increase to 2 × 2 × 1 and 3 × 3 × 1, and the peak shapes and locations tend to be similar to each other. On the other hand, the static dielectric constant $\varepsilon(0)$ increases with the increase of the section size due to the decrease of band gap,[1] as shown in Table S4. The similar phenomenon has been observed in Si_3N_4 films with thickness less than 6 nm, for which the $\varepsilon(0)$ decreases with the decrease of their thickness.[2] From this table, the orientations of nanobelts have an effect on the $\varepsilon(0)$, which decreases in the order of [001], [110] and [100].

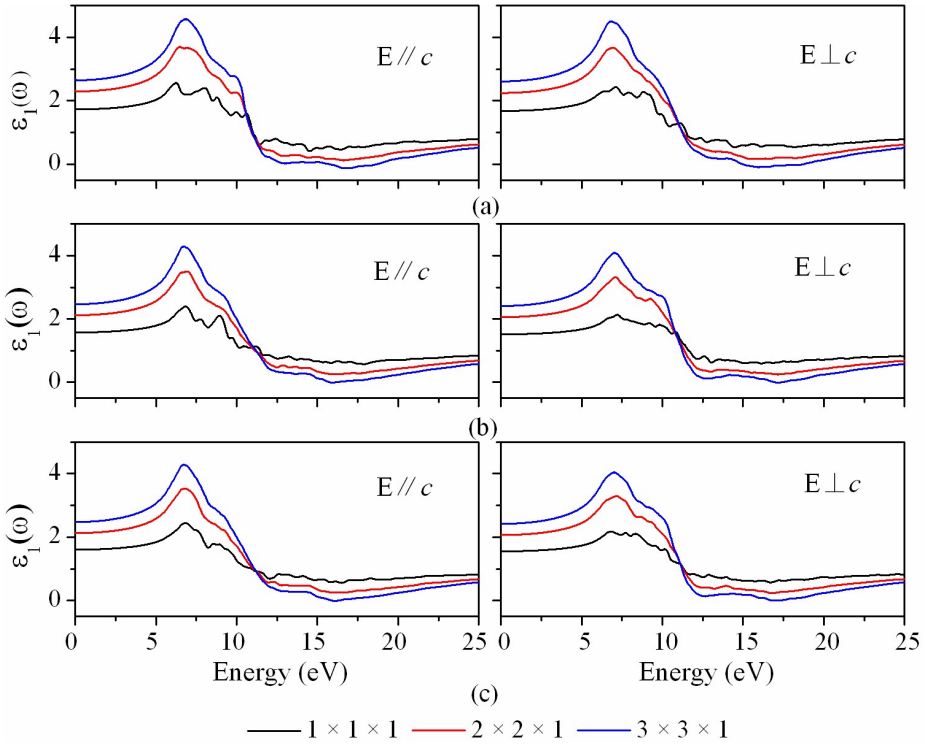

Fig. S7 Real parts $\varepsilon_1(\omega)$ of the dielectric functions of the (a) [001]-, (b) [100]- and (c) [110]-orientated α-Si_3N_4 nanobelts with different supercells.

Table S4 The static dielectric constants $\varepsilon(0)$ of α-Si_3N_4 nanobelts with different orientations and supercells

Incident direction	Supercell	Orientation		
		[001]	[100]	[110]
E // *c*	1 × 1 × 1	1.74	1.58	1.61
	2 × 2 × 1	2.32	2.13	2.14
	3 × 3 × 1	2.69	2.48	2.50
E ⊥ *c*	1 × 1 × 1	1.68	1.52	1.55
	2 × 2 × 1	2.25	2.06	2.07
	3 × 3 × 1	2.62	2.41	2.42

The other static optical parameters of the α-Si_3N_4 nanobelts, including the static reflectivity $R(0)$ and the static refractivity $n(0)$ can be derived from the static dielectric property, as shown in Table S5 and S6, respectively. The changes of these values as the supercells and orientations are similar to those of $\varepsilon(0)$.

Table S5 The static reflectivities $R(0)$ (%) of α-Si_3N_4 nanobelts with different orientations and supercells

Incident direction	Supercell	Orientation		
		[001]	[100]	[110]
E // c	1 × 1 × 1	1.88	1.29	1.40
	2 × 2 × 1	4.31	3.49	3.54
	3 × 3 × 1	5.87	5.00	5.06
E ⊥ c	1 × 1 × 1	1.67	1.08	1.21
	2 × 2 × 1	4.00	3.19	3.24
	3 × 3 × 1	5.58	4.70	4.75

Table S6 The static refractivities $n(0)$ of α-Si_3N_4 nanobelts with different orientations and supercells

Incident direction	Supercell	Orientation		
		[001]	[100]	[110]
E // c	1 × 1 × 1	1.32	1.26	1.27
	2 × 2 × 1	1.52	1.46	1.46
	3 × 3 × 1	1.64	1.58	1.58
E ⊥ c	1 × 1 × 1	1.30	1.23	1.25
	2 × 2 × 1	1.50	1.44	1.44
	3 × 3 × 1	1.62	1.55	1.56

Fig. S8 displays the optical conductivities of α-Si_3N_4 nanobelts with different orientations and supercells. As the section size of α-Si_3N_4 nanobelt increases, the optical conductivity increases. The [001]-orientated α-Si_3N_4 nanobelt with 3 × 3 × 1 supercell possesses the largest conductivity value of $6.0\times10^3\Omega^{-1}\cdot cm^{-1}$ at about 11eV for light polarized parallel to the nanobelt axis. While the supercells increase to 2 × 2 × 1 and 3 × 3 × 1, the number of peaks decreases, and the peak shapes and locations tend to be similar to each other. The main peaks locate at about 8, 11 and 15 eV, which are accord with the imaginary parts $\varepsilon_2(\omega)$ of dielectric functions. Additionally, the minimum photo energies are above 5 eV and red-shifted slightly with the increase of section sizes due to the subtle decrease of band gaps.

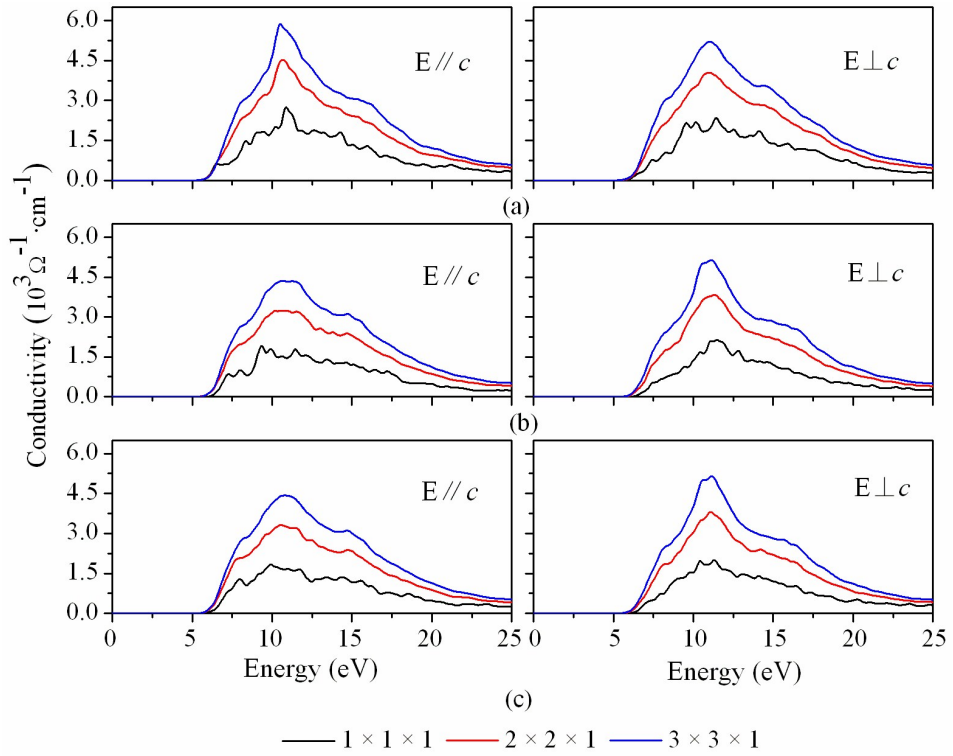

Fig. S8 Optical conductivities of the (a) [001]-, (b) [100]- and (c) [110]-orientated α-Si_3N_4 nanobelts with different supercells.

References

[1] Z. F. Huang, F. Chen, R. Su, Z. H. Wang, J. Y. Li, Q. Shen, L. M. Zhang, *J. Alloy. Compd.*, 2015, **637**, 376-381.

[2] T. A. Pham, T. Li, S. Shankar, F. Gygi, G. Galli, *Appl. Phys. Lett.*, 2010, **96**, 062902.